Communication

Production of Polyhydroxyalkanotes by an Extreme Halophilic Bacterium Halomonas gomseomensis Using Different Carbon Sources

Radamés Tejo-Valencia , José Manuel Cervantes-Uc , Efraín Ramírez-Benitez , Gabriel Lizama-Uc * , Manuel Fortis-Hernández , Edgar Omar Rueda-Puente *

Posted Date: 12 March 2024

doi: 10.20944/preprints202403.0692.v1

Keywords: Bioplastics; Halomonas gomseomensis; Polyhydroxyalkanoates

Article

In-Plane Mechanical Characterization of a Kevlar® Composite

Rene Alejandro Canceco de la Cruz [1], Caleb Carreño Gallardo [1] Alberto Diaz Diaz [1], Luis Adrian Zuñiga Aviles [2], Gabriel Plascencia Barrera [1] and Jose Martin Herrera Ramirez [1,*]

[1] Centro de Investigación en Materiales Avanzados, S.C. (CIMAV), Av. Miguel de Cervantes #120, Complejo Industrial Chihuahua, Chihuahua, Chih. México. C.P. 31136.

[2] Facultad de Medicina, Universidad Autonoma del Estado de México, Toluca, Mexico. C.P. 50180.

* Correspondence: martin.herrera@cimav.edu.mx

Abstract: Polymer-based composites are widely used in the automotive, security, aeronautical and space industries, to mention a few. This is because of their good mechanical properties, which are similar to those of metals but with the attraction of being lightweight. Kevlar® as a reinforcement is extensively used in the security industry owing to its good ballistic properties. This investigation presents the mechanical characterization based on in-plane quasi-static tensile testing of Kevlar® 29/phenolic resin with polyvinyl butyral composite using a universal testing system. The methodology developed for the preparation of coupons is based on pressure, temperature and time. As a result of this work, elastic moduli (E_L and E_T), Poisson's ratio (ν_{LT}), shear modulus (G_{LT}) and strengths (X_T, Y_T, S) were obtained. It is worth mentioning that there is scarce or no characterization of this material in the literature, and those studies that do characterize it do not present the coupon thermoforming conditions or the reasons of the coupon dimensions (width, length and thickness).

Keywords: Kevlar®, Polymer composite; Mechanical properties; Quasi-static tensile test

1. Introduction

Fiber-reinforced composites are now firmly at the forefront of advanced materials and are used in an increasing number of applications, from fishing rods to satellites. Today, the largest use of high-performance composite is in civilian applications, but initially it was military and, in particular, in aerospace structures. The reason for the use of these materials is due to weight savings [1].

The present work consists of the in-plane characterization of a Kevlar® material preimpregnated with phenolic resin with polyvinyl butyral on both sides. As a first stage of this study, it is intended to know the mechanical properties of the in-plane interweaving through tensile tests based on the ASTM D3039/D3039M standard using a universal testing system to acquire the elastic moduli and strengths. The elastic constants obtained from this study will be used for a subsequent improvement study of an antifragment helmet using the finite element method. In the literature, there are studies that can be classified according to the geometry under study, either focused on military helmets or on rectangular geometries subjected to ballistic impact using computational tools such as LS-DYNA® or ABAQUS® (Table 1). The mechanical properties used in this type of works come from the study done by van Hoof in 2000-2001 [2, 3]. The work done by van Hoof was the pioneer in the use of numerical simulations of ballistic impact on reinforcement laminates of Kevlar® 29/phenolic material. In his work he simulated a laminate with rectangular geometry impacted by a projectile fragment; in his numerical simulation he took mechanical properties of Kevlar® from Zhu who characterized the Kevlar® 29/polyester material through quasi-static and dynamic tests in 1981 [4]. From the validation van Hoof didn't observed correlation between the numerical simulation and the ballistic test, therefore a "calibration" of the mechanical properties (strengths) was carried out to force a correlation. From this work, parameters of the Kevlar® material were obtained that are still used today for ballistic studies on combat helmets [5-12], as shown in Table 1.

The methodology used by Zhu [4] to obtain the elastic moduli in the warp and weft directions was through of coupons with intercalated layers at [0°, 90°] obtaining an elastic modulus of 18.5 GPa

 doi:10.20944/preprints202403.0692.v1

for both orthotropy directions, therefore no distinction was made between the principal directions of the material. And, the way in which the shear modulus was characterized is not recommended, since it generates undesirable deformations at the ends of the coupons, so a methodology based on symmetrical laminates is proposed in our work to prevent the coupons from generating moments in the universal testing system grips.

The research presented by Nunes et al. [13] characterized intensively the Kevlar® 29/epoxy composite in-plane through tensile, compression, V-notch rail shear and short beam tests. Also, Scazzosi et al. [14] determined the mechanical properties of Kevlar® 29/epoxy composite in-plane with tensile tests. The research by Gower et al. [15] characterized the Kevlar® 129 through tensile test, but neither the thermoforming conditions nor the dimensions of the coupons are exposed. There are a limited number of works in the literature that characterize the Kevlar® material in the plane.

A woven fabric can be studied as an orthotropic material with 9 elastic constants represented in a matrix of compliances, as shown in Equation (1) [16]. The matrix considers the elastic moduli (E_L, E_T, E_N, G_{LT}, G_{TN}, G_{LN}) and Poisson's ratio (ν_{TL}, ν_{NL}, ν_{NT}). The subscripts L, T and N represents the orthotropic directions of a woven fabric as shown in Figure 1**.** The aim of this work is to characterize the Kevlar® material in the L-T plane.

Table 1. In-plane mechanical properties of Kevlar® found in the literature.

	Rectangular Plate				Helmet		
Mechanical property	**Kevlar 29 / Phenolic**	**Kevlar 29 / Epoxy**	**Kevlar 29 / Epoxy**	**Kevlar 29 / Epoxy**	**Kevlar**	**Kevlar 29**	**Kevlar**
E_L [GPa], Longitudinal elastic modulus	18.5	18.5	7.618	10.06	18	18.5	18.5
E_T [GPa], Transversal elastic modulus	18.5	18.5	11.05	10.06	18	18.5	18.5
ν_{LT}, Poisson's ratio L-T	0.25	0.25	0.18	0.25	0.25	0.25	0.25
G_{LT} [GPa], Shear modulus in L-T plane	0.77	0.77	2.123	0.77	0.77	0.77	0.77
X_T [MPa], Tensile strength in longitudinal direction	555(2)	1850(1)	400	425	555	555	555
Y_T [MPa], Tensile strength in transversal direction	555(2)	1850(1)	530	425	555	555	555
S [MPa], Shear strength in L-T direction	77	77	67	77	77	77	77
Autor	van Hoof [2]	Bresciani et al. [11]	Nunes et al. [13]	Scazzosi et al. [14]	Tan et al. [9]	Caçoilo et al. [8]	Lee et al. [6]

(1) Strength property adopted "initially" in the numerical model for woven Kevlar® by van Hoof [2].
(2) Strength property adopted "finally" in the numerical model for woven Kevlar® by van Hoof [2, 3].

Preprints.org (www.preprints.org) | NOT PEER-REVIEWED | Posted: 12 March 2024 doi:10.20944/preprints202403.0692.v1

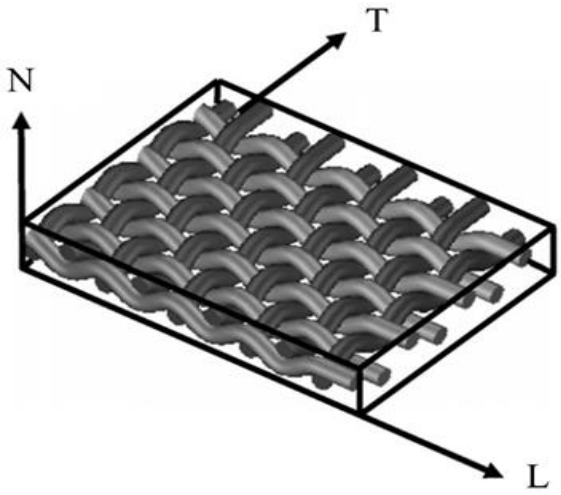

Figure 1. Orthotropic directions of a woven material: longitudinal (L), transversal (T) and normal to the plane L-T (N) [17].

$$\begin{Bmatrix} \varepsilon_L \\ \varepsilon_T \\ \varepsilon_N \\ 2\varepsilon_{TN} \\ 2\varepsilon_{LN} \\ 2\varepsilon_{LT} \end{Bmatrix} = \begin{bmatrix} \frac{1}{E_L} & -\frac{\nu_{TL}}{E_T} & -\frac{\nu_{NL}}{E_N} & 0 & 0 & 0 \\ -\frac{\nu_{LT}}{E_L} & \frac{1}{E_T} & -\frac{\nu_{NT}}{E_N} & 0 & 0 & 0 \\ -\frac{\nu_{LN}}{E_L} & -\frac{\nu_{TN}}{E_T} & \frac{1}{E_N} & 0 & 0 & 0 \\ 0 & 0 & 0 & \frac{1}{G_{TN}} & 0 & 0 \\ 0 & 0 & 0 & 0 & \frac{1}{G_{LN}} & 0 \\ 0 & 0 & 0 & 0 & 0 & \frac{1}{G_{LT}} \end{bmatrix} \begin{Bmatrix} \sigma_L \\ \sigma_T \\ \sigma_N \\ \sigma_{TN} \\ \sigma_{LN} \\ \sigma_{LT} \end{Bmatrix} \quad (1)$$

or, in brief: $\varepsilon = c \cdot \sigma$, where ε represents the vector of strains, C is the matrix of compliances in the orthotropic direction and σ is the vector of stresses. By symmetry: $\nu_{TL} = \nu_{LT}\frac{E_T}{E_L}$, $\nu_{NL} = \nu_{LN}\frac{E_N}{E_L}$, $\nu_{NT} = \nu_{TN}\frac{E_N}{E_T}$. The principal material directions of the individual layers within the laminate will not necessarily coincide with the global laminate axis. The stiffness R′ and compliance C′ matrix for each layer must be expressed within the global material axis of the laminate using the following transformations given in Equation (2) and Equation (3).

$$R' = O_\sigma \cdot R \cdot O_\varepsilon^{-1} = O_\sigma \cdot R \cdot O_\sigma^t \quad (2)$$

$$C' = O_\varepsilon \cdot C \cdot O_\sigma^{-1} = O_\varepsilon \cdot C \cdot O_\varepsilon^t \quad (3)$$

where O_σ and O_ε represent the rotation matrices used to obtain the compliance matrix in the global axis system, according to Equation (4) and Equation (5), respectively.

$$O_\sigma = \begin{pmatrix} c^2 & s^2 & 0 & 0 & 0 & -2cs \\ s^2 & c^2 & 0 & 0 & 0 & 2cs \\ 0 & 0 & 1 & 0 & 0 & 0 \\ 0 & 0 & 0 & c & s & 0 \\ 0 & 0 & 0 & -s & c & 0 \\ cs & -cs & 0 & 0 & 0 & c^2 - s^2 \end{pmatrix} \quad (4)$$

$$O_\varepsilon = \begin{pmatrix} c^2 & s^2 & 0 & 0 & 0 & -cs \\ s^2 & c^2 & 0 & 0 & 0 & cs \\ 0 & 0 & 1 & 0 & 0 & 0 \\ 0 & 0 & 0 & c & s & 0 \\ 0 & 0 & 0 & -s & c & 0 \\ 2cs & -2cs & 0 & 0 & 0 & c^2 - s^2 \end{pmatrix} \quad (5)$$

where c=cos θ and s=sin θ. Finally, the vector of stresses σ' and strains ε' in the global axis system is determined by Equation (6) and Equation (7), respectively.

$$\sigma' = R' \cdot \varepsilon' \quad (6)$$

 doi:10.20944/preprints202403.0692.v1

$$\varepsilon' = C' \cdot \sigma' \tag{7}$$

For a plane stresses study the Equation (1) become in Equation (8). In the first stage of this work the composite material was characterized in-plane using tensile tests. According with the matrix of compliances of Equation (8) it is required to know the elastic moduli (E_L and E_T,), shear modulus (G_{LT}), Poisson's ratio (ν_{TL}) and strengths (X_T, Y_T and S).

$$\begin{Bmatrix} \varepsilon_L \\ \varepsilon_T \\ 2\varepsilon_{LT} \end{Bmatrix} = \begin{bmatrix} \frac{1}{E_L} & -\frac{\nu_{TL}}{E_T} & 0 \\ -\frac{\nu_{LT}}{E_L} & \frac{1}{E_T} & 0 \\ 0 & 0 & \frac{1}{G_{LT}} \end{bmatrix} \begin{Bmatrix} \sigma_L \\ \sigma_T \\ \sigma_{LT} \end{Bmatrix} \tag{8}$$

2. Materials and Methods

Figure 2a shows one sheet of Kevlar® 29/phenolic resin with polyvinyl butyral used for the production of antifragment helmets. This material is preimpregnated with resin on both sides. As shown in the image, the material has horizontal and vertical cuts, since it was prepared for using in the manufacture of helmets; these cuts limited the coupons extraction. For the development of this in-plane testing program, straight geometries based on the ASTM D3039/D3039M [18] standard were implemented to determine elastic moduli (E_L, E_T), shear modulus (G_{LT}), Poisson's ratio (ν_{LT}) and strengths (X_T, Y_T, S) through tensile tests. Straight coupons are beneficial when a water jet cutting machine is not available, facilitating the cutting process of each layer by using sheet metal cutting scissors. A Hitachi® scanning electron microscope model SU3500 was used to identify the orthotropic directions (Figure 2b); a repetitive unit size of 3 mm was observed, with the yarn width being greater in the longitudinal direction than in the transversal direction. The orthotropic directions of each sheet were identified in order to produce coupons with the properly identified directions.

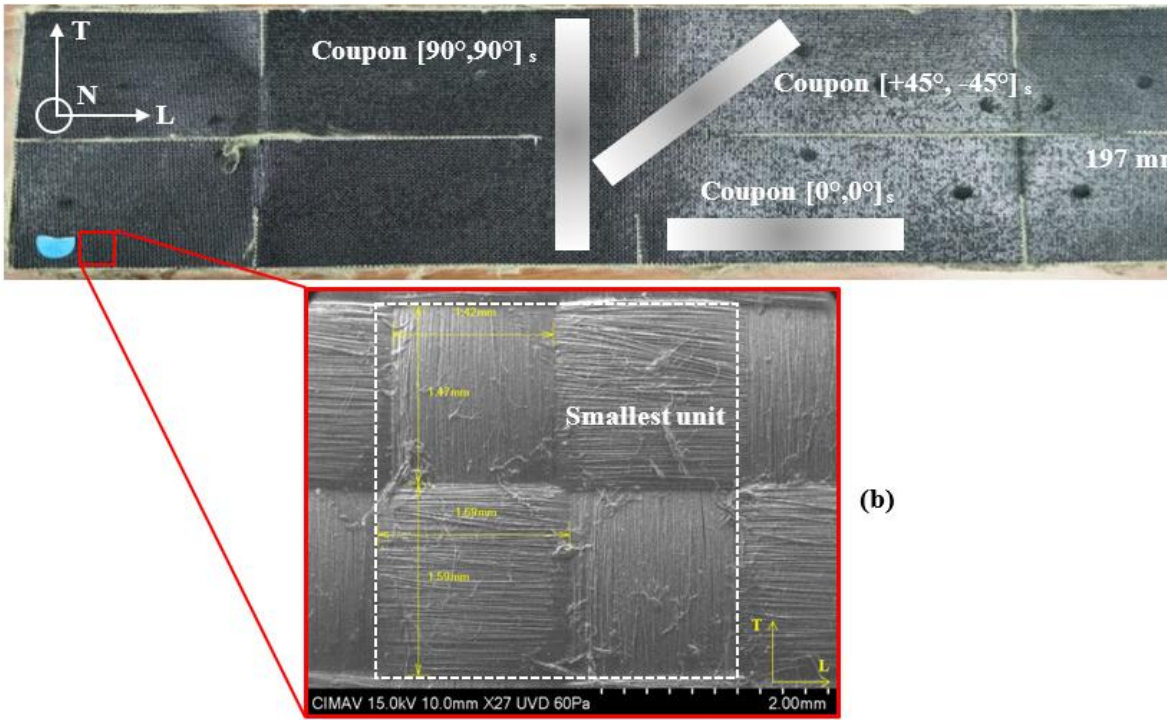

Figure 2. (**a**) As-received Kevlar® 29/phenolic resin with polyvinyl butyral material indicating where the coupons were taken from, (**b**) Scanning electron microscopy image for the identification of the orthotropic directions.

Jones proposed to determine the shear modulus G_{LT} using a tensile test instead of using the Iosipescu method, which requires special grips that are not available in most laboratories. To perform

 doi:10.20944/preprints202403.0692.v1

this test, the layers are required to be oriented at 45° and, by Equation (9) it is possible to determine the shear modulus in the G_{LT} plane; E_x is the elastic modulus with the material oriented at 45° [19]. The method proposed by Jones generates angular strains at the end of the coupons edges when the ends of the laminate are free to deform, as shown on the left side of Figure 3. However, if the ends of coupon are clamped, this causes the coupon to twist and generates moments at gripping points, as shown on the right side of Figure 3.

$$G_{LT} = \left(\frac{1}{\frac{4}{E_x} - \frac{1}{E_L} + \frac{2\upsilon_{LT}}{E_L} - \frac{1}{E_T}} \right) \tag{9}$$

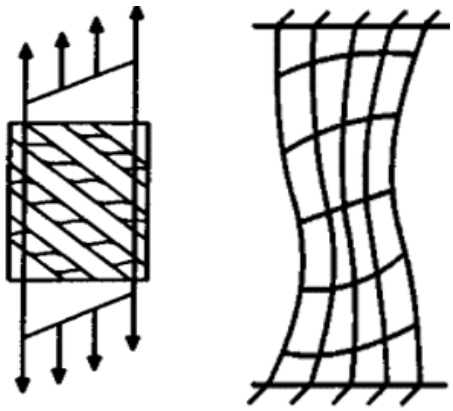

Figure 3. Deformation of a unidirectional reinforced laminate loaded at 45° to the fibers [19].

An alternative procedure to the Jones' equation to obtain the shear modulus G_{LT} using straight coupons at $[+45°,-45°]_s$ is presented below as shown in Figure 5 by performing tensile tests using a universal testing system. This methodology avoids deformations such as those shown in Figure 3.

In the case of a laminate, the total force and moment resultants are obtained by adding the effects of all layers in a single-layer element, as shown in Figure 4.

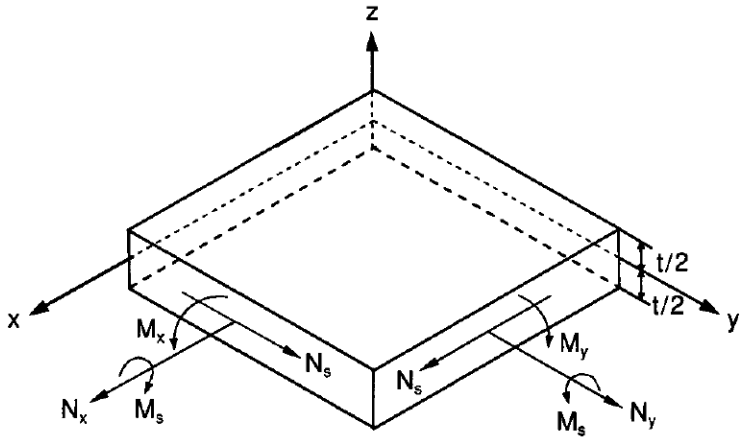

Figure 4. Element of single layer with resultant forces and moments [16].

The force-deformation relationship and the moment-deformation relationship are described by Equation (10) and Equation (11), respectively [16]:

$$\begin{bmatrix} N_x \\ N_y \\ N_s \end{bmatrix} = \begin{bmatrix} A_{xx} & A_{xy} & A_{xs} \\ A_{yx} & A_{yy} & A_{ys} \\ A_{sx} & A_{sy} & A_{ss} \end{bmatrix} \begin{bmatrix} \varepsilon_x \\ \varepsilon_y \\ \gamma_s \end{bmatrix} + \begin{bmatrix} B_{xx} & B_{xy} & B_{xs} \\ B_{yx} & B_{yy} & B_{ys} \\ B_{sx} & B_{sy} & B_{ss} \end{bmatrix} \begin{bmatrix} \kappa_x \\ \kappa_y \\ \kappa_s \end{bmatrix} \tag{10}$$

 doi:10.20944/preprints202403.0692.v1

$$\begin{bmatrix} M_x \\ M_y \\ M_s \end{bmatrix} = \begin{bmatrix} B_{xx} & B_{xy} & B_{xs} \\ B_{yx} & B_{yy} & B_{ys} \\ B_{sx} & B_{sy} & B_{ss} \end{bmatrix} \begin{bmatrix} \varepsilon_x \\ \varepsilon_y \\ \gamma_s \end{bmatrix} + \begin{bmatrix} D_{xx} & D_{xy} & D_{xs} \\ D_{yx} & D_{yy} & D_{ys} \\ D_{sx} & D_{sy} & D_{ss} \end{bmatrix} \begin{bmatrix} \kappa_x \\ \kappa_y \\ \kappa_s \end{bmatrix} \quad (11)$$

where N_x, N_y are the normal forces per unit length, N_s is the shear force per unit length, M_x, M_y are the bending moments per unit length and M_s is the twisting moment per unit length [16].

Equation (10) and Equation (11) can be combined into one general expression that briefly relates the in-plane forces and moments to the reference plane strains and curvatures, as indicated by Equation (12):

$$\begin{bmatrix} N \\ M \end{bmatrix} = \begin{bmatrix} A & B \\ B & D \end{bmatrix} \begin{bmatrix} \varepsilon^{\circ} \\ \kappa \end{bmatrix} \quad (12)$$

The above relations are expressed in terms of three laminate stiffness matrices, [A], [B], and [D], which are functions of the thickness, material properties and stacking sequence of the individual layers. [A] is the extensional stiffness matrix expressed by Equation (13), which relates in-plane forces to in-plane strains, [B] is the coupling stiffness matrix expressed by Equation (14), which relates in-plane forces to curvatures and moments to in-plane strains. [D] is the bending laminate stiffness matrix expressed by Equation (15), which relates moments to curvatures [16].

$$A = \sum_{i=1}^{n} h_i \, (C_i')^{-1} \quad (13)$$

$$B = \sum_{i=1}^{n} e_i \, h_i (C_i')^{-1} \quad (14)$$

$$D = \sum_{i=1}^{n} \left[e_i (h_i)^2 + \frac{e^3}{12} \right] (C_i')^{-1} \quad (15)$$

where e_i represents the vector of thickness for each layer and C_i' is the matrix of compliances in the global system. As in symmetric laminates B=0, therefore is no coupling between in-plane loading and out-of-plane deformation (curvatures) and between bending and twisting moments and in-plane deformation. These laminates exhibit no distortion or warpage after fabrication and are easier to analyze. Therefore, Equation (10) and Equation (11) become Equation (16) and Equation (17), respectively:

$$\begin{bmatrix} N_x \\ N_y \\ N_s \end{bmatrix} = \begin{bmatrix} A_{xx} & A_{xy} & A_{xs} \\ A_{yx} & A_{yy} & A_{ys} \\ A_{sx} & A_{sy} & A_{ss} \end{bmatrix} \begin{bmatrix} \varepsilon_x \\ \varepsilon_y \\ \gamma_s \end{bmatrix} \quad (16)$$

$$\begin{bmatrix} M_x \\ M_y \\ M_s \end{bmatrix} = \begin{bmatrix} D_{xx} & D_{xy} & D_{xs} \\ D_{yx} & D_{yy} & D_{ys} \\ D_{sx} & D_{sy} & D_{ss} \end{bmatrix} \begin{bmatrix} \kappa_x \\ \kappa_y \\ \kappa_s \end{bmatrix} \quad (17)$$

When an axial load N_X is applied through a universal testing system to a coupon with a configuration of 4 layers $[+45°,-45°]_s$ and according to Equation (16) $N_y=N_s=0$ and $\gamma_s=0$ (the edges remain straight), and ε_x and ε_y are different of zero. Inverting matrix A of Equation (16) yields Equation (18) to obtain ε_x.

$$\varepsilon_x = \frac{\{N_x[E_L^2 + E_L E_T + 4E_L G_{LT} + 2E_L E_T \nu_{LT} - 4E_T G_{LT} \nu_{LT}^2]\}}{[16E_L e(E_L G_{LT} + E_T G_{LT} + 2E_T G_{LT} \nu_{LT})]} \quad (18)$$

where e is the thickness of each layer considering in this case that each layer has the same thickness. $\sigma_x = \frac{N_x}{4e}$ represents the average stress of all layers because the stress change from layer to layer and $E_{\mp 45\_S} = \frac{\sigma_x}{\varepsilon_x}$, thus obtaining the shear modulus G_{LT} (Equation (19)).

$$G_{LT} = \frac{E_{\mp 45\_S} E_L (E_L + E_T + 2E_T \nu_{LT})}{4\left[E_L (E_L + E_T + 2E_T \nu_{LT}) + E_{\mp 45_S} (E_T \nu_{LT}^2 - E_L)\right]} \quad (19)$$

If E_L=E_T Equation (19) become in Equation (20).

$$G_{LT} = \frac{2E_{\mp 45\_S} E_L (E_L + E_T \nu_{LT})}{4\left[2E_L (E_L + E_L \nu_{LT}) + E_{\mp 45_S} (E_L \nu_{LT}^2 - E_L)\right]} \quad (20)$$

Figure 5 shows the coupon geometry, as well as the dimensions and number of locally thermoformed tabs at the coupons ends, in order to protect the material from the universal machine

 doi:10.20944/preprints202403.0692.v1

grips and ensure the coupon breakage away from the grips. A coupon width of 32 mm was considered taking into account that to obtain the Poisson's ratio ν_{LT} a strain gage has to be positioned transversely to the coupon. The material was cut according to the orthotropic directions, as shown in Figure 1. The coupon length used was 197 mm, which represents the maximum length that was possible to obtain from the as-received material. For the tabs, it was proposed to make a smooth transition in the thickness of the coupons and thus avoid a pronounced concentration of stresses.

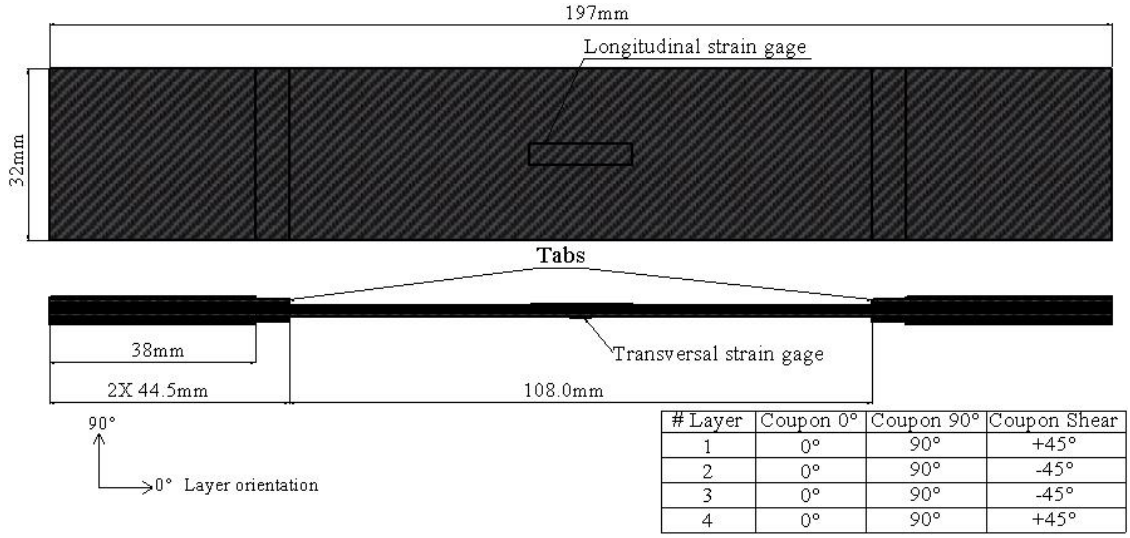

# Layer	Coupon 0°	Coupon 90°	Coupon Shear
1	0°	90°	+45°
2	0°	90°	-45°
3	0°	90°	-45°
4	0°	90°	+45°

Figure 5. Geometry of coupons for the in-plane characterization.

The grid length in the longitudinal direction of the gage is 12.7 mm which is large enough to cover 4.2 repeat units of the woven fabric and thus to obtain a correct measurement of the Poisson's ratio ν_{TL}. During the tensile test, large strains are expected, so EP type gages (Micro-Measurements® EP-08-500GB-120) which are for applications of up to +/-20%, were selected. Finally, a gage was selected for a resistance of 120 Ω, which the equipment can read.

A mold and cover were designed and fabricated from 6.35 cm x 25.4 cm x 1.27 cm AISI 1018 steel plates. The thickness of 1.27 cm was chosen to avoid buckling in the middle of the plate during the mold manufacture. Figure 6a shows the stacking of resin-preimpregnated Kevlar® layers; the use of Teflon® paper was necessary to prevent the sample from sticking to the mold. Figure 6b shows the closed mold and Figure 6c shows a Carver® 4122 Manual Heated Press (10 t) where the coupon thermoforming process was performed. The thermoforming conditions were 192 °C with a compression load of 6.5 t for 10.5 min, which were based on the manufacturing conditions of the antifragment helmets. The compression load and time conditions applied to the tabs were reduced to 2 t and 3 min, respectively, to avoid a local reduction in the thickness of the coupons ends.

 doi:10.20944/preprints202403.0692.v1

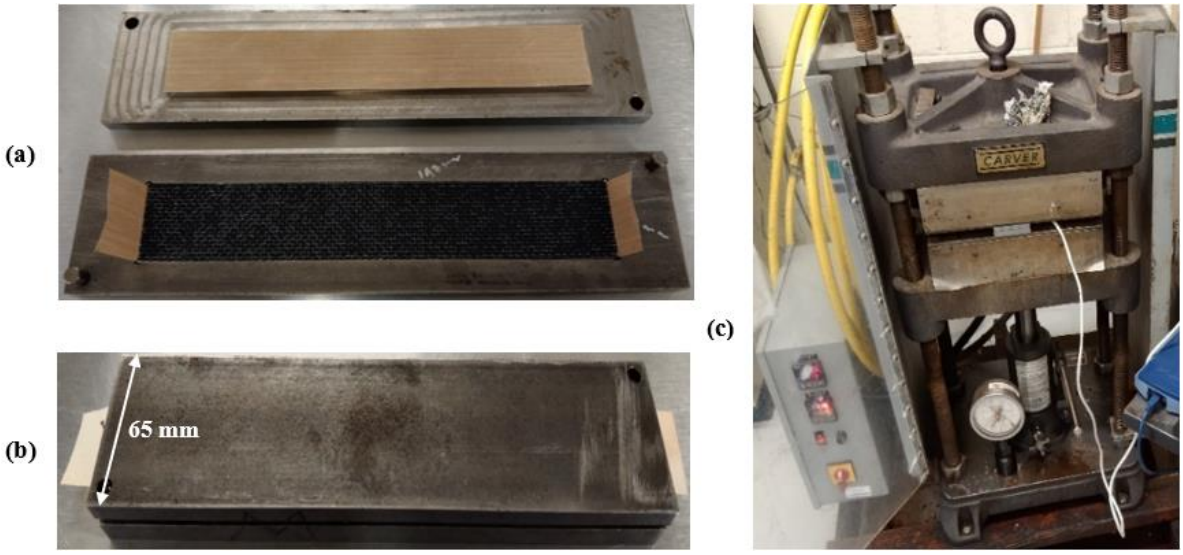

Figure 6. (**a**) Stacking of layers in the mold, (**b**) Closing of the mold prior to thermoforming of coupon and (**c**) Carver® 4122 Manual Heated Press.

For the tensile test, an Instron® 3382 universal testing system was used (Figure 7). A head displacement rate of 2 mm/min (0.019 min-1) was used, according to the ASTM D3039/D3039M standard [18]. Mechanical wedge-action grips type 2716-003 were used.

Figure 7. Tensile test performed on a coupon instrumented with strain gages using an Instron® 3382 universal testing system.

3. Results and Discussion

Figure 8 shows the tensile stress-strain curves of four coupons tested at 0° (longitudinal direction). It is worth mentioning that three of them (EL-2, EL-3, EL-4) did not reach the strength and strain of coupon EL-1 due to the debonding of their tabs; however, the four coupons performed similarly in the 0-2% strain range, which was adequate to calculate the longitudinal elastic modulus (E_L = 11.78 ± 1.07 GPa). Two additional coupons (EL-5, EL-6) with no strain gage instrumentation were tested to determine a suitable strength (X_T = 648.33 ± 56.31 MPa) (Figure 9). Figure 11 shows the coupon appearance after these tensile tests.

 doi:10.20944/preprints202403.0692.v1

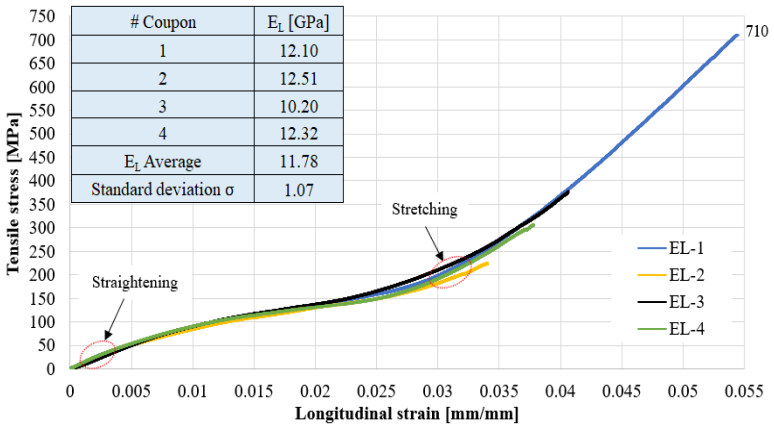

# Coupon	E_L [GPa]
1	12.10
2	12.51
3	10.20
4	12.32
E_L Average	11.78
Standard deviation σ	1.07

Figure 8. Tensile stress-strain curves of coupons tested at 0°. Strain measured with strain gages.

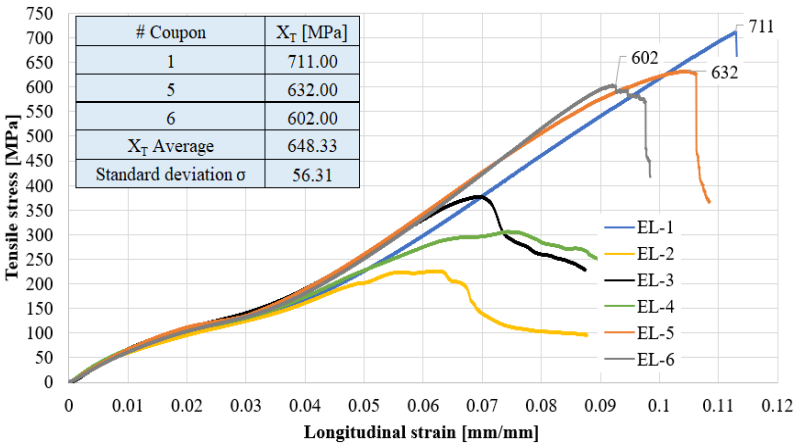

# Coupon	X_T [MPa]
1	711.00
5	632.00
6	602.00
X_T Average	648.33
Standard deviation σ	56.31

Figure 9. Tensile stress-strain curves of coupons tested at 0°. Coupons EL-5 and EL-6 were added. Strain measured with the universal machine.

Figure 10 shows the longitudinal strain-transversal strain curves of the coupons tested in tension at 0°, from which the Poisson's ratio ($\nu_{LT} = 0.29 \pm 0.06$) was calculated.

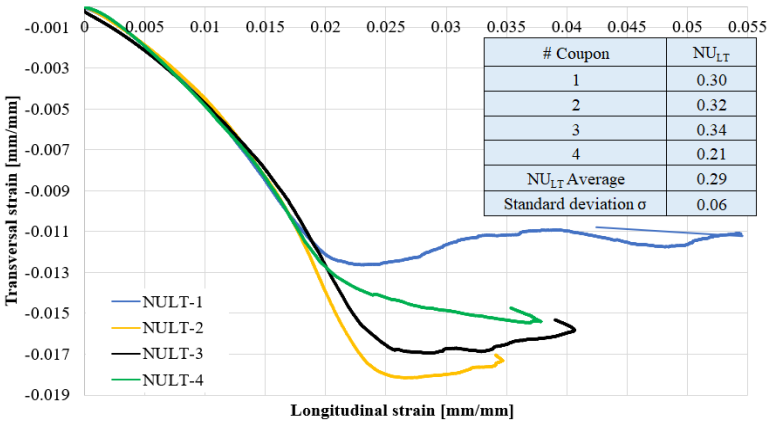

# Coupon	NU_{LT}
1	0.30
2	0.32
3	0.34
4	0.21
NU_{LT} Average	0.29
Standard deviation σ	0.06

Figure 10. Poisson's ratio ν_{LT} of coupons tested in tension at 0°. Strain measured with strain gages.

 doi:10.20944/preprints202403.0692.v1

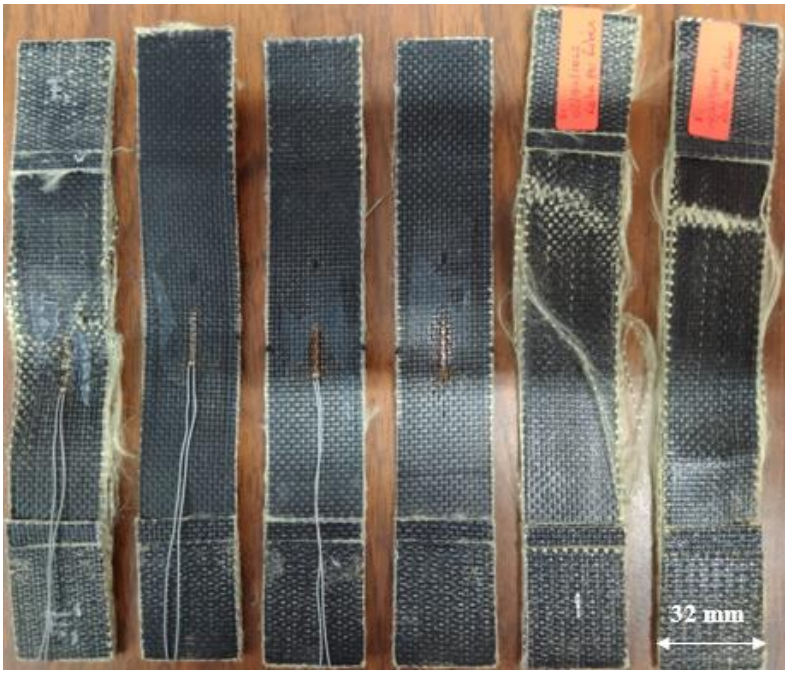

Figure 11. Condition of coupons after the tensile test at 0°.

Figure 12 shows the tensile stress-strain curves of four coupons tested at 90° (transversal direction). Due to the debonding of one of the tabs of the coupon ET-3, it did not reach the strength and deformation of the other three coupons; however, the four coupons performed similarly in the 0-2% strain range, which was adequate to calculate the transversal elastic modulus (E_T = 15.38 ± 1.34 GPa). The strength calculation (Y_T = 659.57 ± 20.42 MPa) was made excluding coupon ET-3. Figure 13 shows the coupons appearance after these tensile tests.

Experimental characterization of the stress-strain behavior of the coupons in the 0° and 90° directions revealed two distinct slopes; see Figure 8 and Figure 12. The first slope corresponds to the straightening, and the second to the stretching of the yarns until the rupture; this behavior was noted by Gower [15].

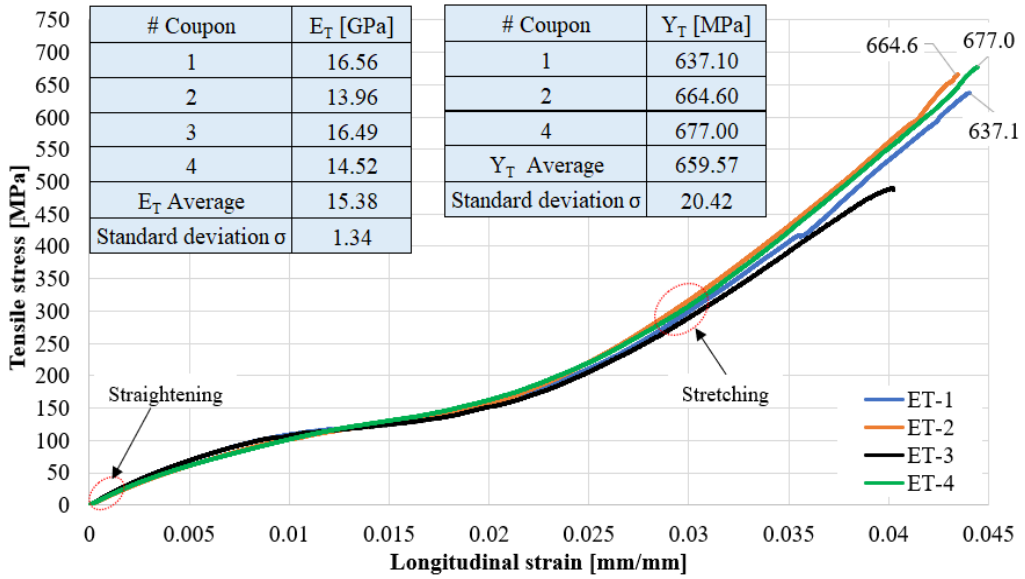

Figure 12. Tensile stress-strain curves of coupons tested at 90°. Strain measured with strain gages.

 doi:10.20944/preprints202403.0692.v1

Figure 13. Condition of coupons after the tensile tests at 90°.

According to this study, the interwoven material is stiffer in the transversal direction than in the longitudinal direction because the former corresponds to the warp direction of the woven fabric; the orthotropic directions of the material were defined in Figure 2. This difference between E_L and E_T was reported by Ito, who attributed it to the tension control during the weaving manufacturing process [20]. Indeed, they observed that the yarns in the warp direction were almost straight, while in the weft direction the yarns waved above and below the warp yarns; gives rise to a small slope or elastic modulus due to the straightening of the yarns.

Figure 14 shows the tensile stress-strain curve of coupons oriented at $[+45°,-45°]_s$. It was not possible to determine the shear strength of the material from these curves because the tabs of all coupons were debonded. Despite this, it was feasible to calculate the elastic modulus in this direction ($E_{\mp 45\_S}$ = 2.82 ± 0.21 GPa), as shown in Figure 15. Figure 16 shows the coupons appearance after these tensile tests. As can be seen, the end edges of the coupons remained straight because symmetry was used in the laminate, avoiding twisting of the coupons (right side of Figure 3). A high longitudinal strain of about 38% (Figure 14) was calculated because a laminate with the material oriented at 45° has the lowest stiffness, as can be seen graphically in Figure 17. Since E_L, E_T, $E_{\mp 45\_S}$ and ν_{LT} were already obtained, it is possible to calculate the shear modulus through Equation (19), which gave a value of G_{LT} = 0.717 GPa. Tsai-Hill failure criterion was used through Equation (21) to determinate a shear strength considering a minimum longitudinal strength of 80 MPa, Figure 14. The Tsai-Hill criterion compares the stresses on the orthotropy system with their corresponding strength direction. The stresses on the orthotropy direction are calculated with the theory of classical laminate model applying loads in the global system, Figure 4. The minimum shear strength obtained was of S = 40 MPa [19, 21].

$$\left(\frac{\sigma_L}{X_T}\right)^2 - \frac{\sigma_L \sigma_T}{(X_T)^2} + \left(\frac{\sigma_T}{Y_T}\right)^2 + \left(\frac{\sigma_{LT}}{S}\right)^2 \geq 1 \qquad (21)$$

Preprints.org (www.preprints.org) | NOT PEER-REVIEWED | Posted: 12 March 2024 doi:10.20944/preprints202403.0692.v1

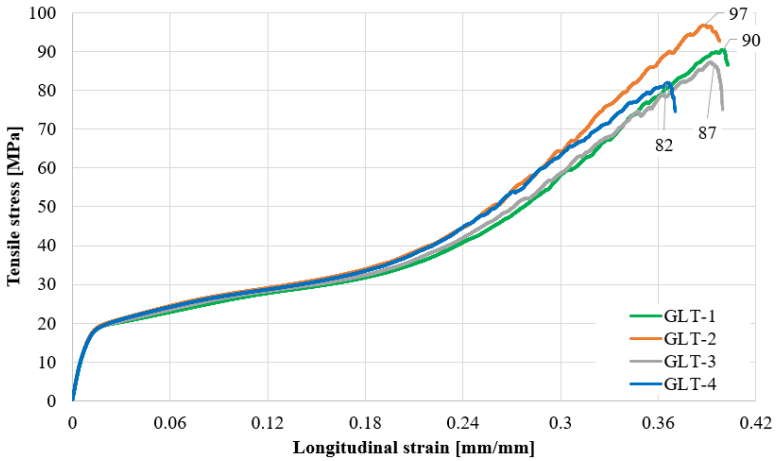

Figure 14. Tensile stress-strain curves of coupons tested at [+45°,-45°]s. Strain measured with universal machine.

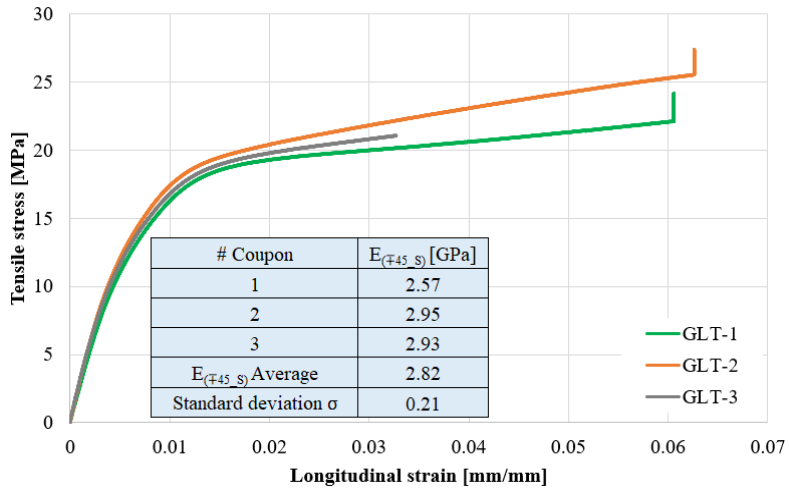

# Coupon	$E_{(\mp 45\_S)}$ [GPa]
1	2.57
2	2.95
3	2.93
$E_{(\mp 45\_S)}$ Average	2.82
Standard deviation σ	0.21

Figure 15. Tensile stress-strain curves of coupons tested at [+45°, -45°]s. Strain measured with strain gages.

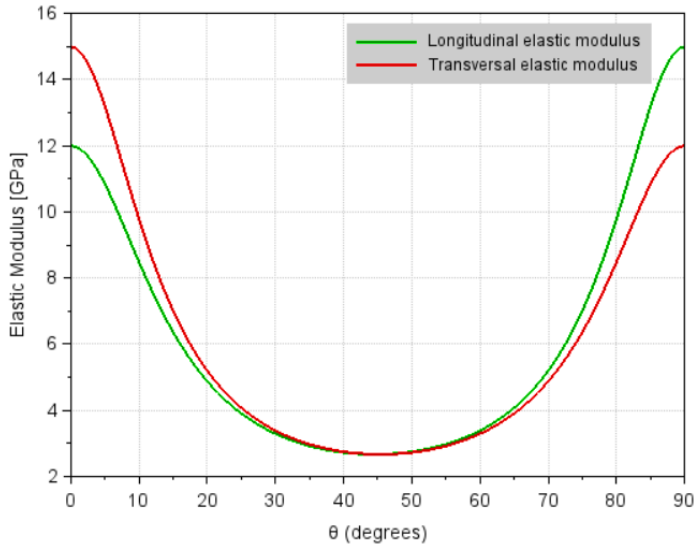

Figure 16. Evolution of the elastic moduli as a function of the laminate orientation.

 doi:10.20944/preprints202403.0692.v1

Figure 17. Condition of coupons after the tensile tests at $[+45°, -45°]_s$.

In Figure 18 is presented a micrography obtained with a digital microscope Keyence® model VHX-7000 of a damaged coupon far from the rupture region but close to the tab, have been found evidence of delamination.

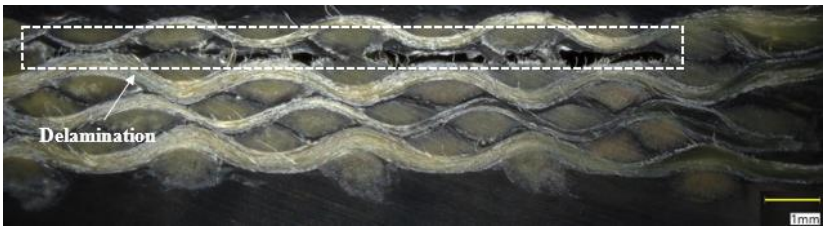

Figure 18. Micrography of a damaged coupon using a digital microscope Keyence® model VHX-7000.

Table 2 summarizes the mechanical properties obtained in present study, which are compared with other results found in the literature. As can be seen, both the elastic moduli and strengths are of the same order of magnitude. However, a very noticeable difference is observed in the shear modulus, which is attributed to the fact that those authors calculated it using the Jones' methodology, with the drawbacks described above.

 doi:10.20944/preprints202403.0692.v1

Table 2. Mechanical properties of Kevlar® composite obtained in this study.

Property	Present work	van Hoof & Zhu et al. [2, 4]	Scazzosi et al. [14]	Nunes et al. [13]
Longitudinal elastic modulus, E_L [GPa]	11.78 (Weft direction)	18.50	10.06	7.618
Transversal elastic modulus, E_T [GPa]	15.38 (Warp direction)	18.50	10.06	11.05
Poisson's ratio, ν_{LT}	0.29	0.25	0.25	0.18
Shear modulus, G_{LT} [GPa]	0.717	0.77	0.77	2.123
Longitudinal Tensile strength, X_T [MPa]	648.33	555.00	425.00	400.00
Transversal Tensile strength, Y_T [MPa]	659.57	555.00	425.00	530.00
Shear strength, S [MPa]	>40.00	77.00	77.00	67.00

4. Conclusions

a) A detailed methodology for the in-plane mechanical characterization of a Kevlar® composite based on quasi-static tensile tests was presented.

b) An alternative to the Jones' method for the shear modulus calculation was proposed, which avoids the moment generation in the grips and prevents the coupon from twisting.

c) As was observed in the tests, there were debonding of the tabs, therefore; a time sweep study was performed at 192 °C using a TA® Instruments RSA3 DMA System (dynamic-mechanical analyzer) on a rectangular layer of 12 mm X 55 mm by a three-point bending test to observe whether the 3 min given to the tabs were sufficient to adhere to the main body of the coupon. Figure 19 shows the storage modulus (E') observing that at a time of 328 s the stiffness remains stable; therefore the 3 min time applied for the thermoforming of the tabs is not enough, at least 6 min must be applied for the local thermoforming of the tabs to avoid debonding of the tabs during the tensile tests.

Author Contributions: Methodology, Rene Alejandro Canceco-de la Cruz; Resources, Caleb Carreño-Gallardo and Luis Adrian Zuñiga-Aviles; Supervision, Alberto Diaz Díaz, Gabriel Plascencia-Barrera and Jose Martin Herrera-Ramirez. All authors have read and agreed to the published version of the manuscript.

Funding: This research received no external funding.

Data Availability Statement: Data are contained within the article.

Acknowledgments: RACC thanks CONAHCYT for his scholarship (grant number 347734). Thanks are due to K. Campos Venegas, E. Ivonne Lopez Martínez, M.E. Mendoza Duarte, I.A. Estrada Moreno, J.E. Ledezma Sillas and R. Castañeda Balderas for the shared expertise and technical support.

Conflicts of Interest: The authors declare no conflicts of interest.

 doi:10.20944/preprints202403.0692.v1

Appendix A

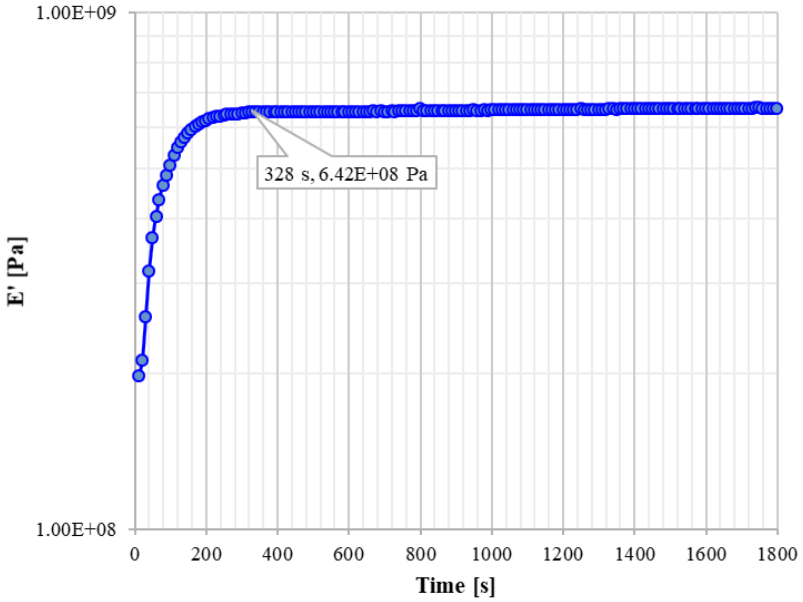

Figure A1. Time sweep obtained with a TA® Instruments RSA3 DMA System.

References

1. A.R. Bunsell, S.J., A. Thionnet, *Fundamentals Of Fibre Reinforced Composite Materials*. 2020.
2. Hoof, J.v., *Modelling of impact induced delamination in composite materials*. 1999, Ottawa-Carleton Institute for Mechanical and Aerospace Engineering.
3. Hoof, J.v., et al. *Numerical head and composite helmet models to predict blunt trauma*. 2001.
4. Guoqi, Z., W. Goldsmith, and C.H. Dharan, *Penetration of laminated Kevlar by projectiles—I. Experimental investigation.* International Journal of Solids and Structures, 1992. **29**(4): p. 399-420.
5. Moure-Guardiola, C., et al., *Evaluation of Combat Helmet Behavior under Blunt Impact.* Applied Sciences, 2020. **10**(23): p. 8470.
6. Lee, H. and S.W. Gong, *Finite element analysis for the evaluation of protective functions of helmets against ballistic impact.* Computer methods in biomechanics and biomedical engineering, 2010. **13**: p. 537-50.
7. Palta, E., H. Fang, and D.C. Weggel, *Finite element analysis of the Advanced Combat Helmet under various ballistic impacts.* International Journal of Impact Engineering, 2018. **112**: p. 125-143.
8. Caçoilo, A., et al., *Modelling ballistic impact on military helmets: The relevance of projectile plasticity.* Defence Technology, 2021. **17**(5): p. 1699-1711.
9. Tan, L.B., et al., *Performance of an advanced combat helmet with different interior cushioning systems in ballistic impact: Experiments and finite element simulations.* International Journal of Impact Engineering, 2012. **50**: p. 99-112.
10. Palomar, M., et al., *Relevant factors in the design of composite ballistic helmets.* Composite Structures, 2018. **201**: p. 49-61.
11. Bresciani, L.M., et al., *Experimental tests and numerical modelling of ballistic impacts against Kevlar 29 plain-woven fabrics with an epoxy matrix: Macro-homogeneous and Meso-heterogeneous approaches.* Composites Part B: Engineering, 2016. **88**: p. 114-130.
12. Manes, A., L.M. Bresciani, and M. Giglio, *Ballistic Performance of Multi-layered Fabric Composite Plates Impacted by Different 7.62mm Calibre Projectiles.* Procedia Engineering, 2014. **88**: p. 208-215.
13. Nunes, S.G., et al., *Influence of projectile and thickness on the ballistic behavior of aramid composites: Experimental and numerical study.* International Journal of Impact Engineering, 2019. **132**: p. 103307.
14. Scazzosi, R., et al., *Two different modelling approaches for fabric composites subjected to ballistic impact.* IOP Conference Series: Materials Science and Engineering, 2018. **406**: p. 012051.
15. Gower, H.L., D.S. Cronin, and A. Plumtree, *Ballistic impact response of laminated composite panels.* International Journal of Impact Engineering, 2008. **35**(9): p. 1000-1008.
16. Daniel, I.M., *Engineering mechanics of composite materials*. 2006.
17. Daniel, I.M., J.-J. Luo, and P.M. Schubel, *Three-dimensional characterization of textile composites.* Composites Part B: Engineering, 2008. **39**(1): p. 13-19.

 doi:10.20944/preprints202403.0692.v1

18. D3039/D3039M, *Standard test method for tensile properties of polymer matrix composite materials*, in *ASTM International: West Conshohocken, PA*. 2017.
19. Jones, R.M., *Mechanics of composite materials*. 1999.
20. Ito, M. and T.-W. Chou, *An Analytical and Experimental Study of Strength and Failure Behavior of Plain Weave Composites.* Journal of Composite Materials, 1998. **32**(1): p. 2-30.
21. Alberto Diaz Diaz, J.-F.C., Alain Ehrlacher, *MAC LAM - Mechanical Analysis of Composites and LAMinates*. 2004.